© 2015. Published by The Company of Biologists Ltd | Journal of Experimental Biology (2015) 218, 3487-3498 doi:10.1242/jeb.123539

RESEARCH ARTICLE

A crayfish molar tooth protein with putative mineralized exoskeletal chitinous matrix properties

Jenny Tynyakov[1,2], Shmuel Bentov[1,2], Shai Abehsera[1], Galit Yehezkel[3], Ziv Roth[1], Isam Khalaila[3], Simy Weil[1], Amir Berman[3], Inbar Plaschkes[2], Moshe Tom[4], Eliahu D. Aflalo[1,2] and Amir Sagi[1,2,*]

ABSTRACT

Some crustaceans possess exoskeletons that are reinforced with calcium carbonate. In the crayfish *Cherax quadricarinatus*, the molar tooth, which is part of the mandibular exoskeleton, contains an unusual crystalline enamel-like apatite layer. As this layer resembles vertebrate enamel in composition and function, it offers an interesting example of convergent evolution. Unlike other parts of the crayfish exoskeleton, which is periodically shed and regenerated during the molt cycle, molar mineral deposition takes place during the pre-molt stage. The molar mineral composition transforms continuously from fluorapatite through amorphous calcium phosphate to amorphous calcium carbonate and is mounted on chitin. The process of crayfish molar formation is entirely extracellular and presumably controlled by proteins, lipids, polysaccharides, low-molecular weight molecules and calcium salts. We have identified a novel molar protein termed Cq-M15 from *C. quadricarinatus* and cloned its transcript from the molar-forming epithelium. Its transcript and differential expression were confirmed by a next-generation sequencing library. The predicted acidic pI of Cq-M15 suggests its possible involvement in mineral arrangement. *Cq-M15* is expressed in several exoskeletal tissues at pre-molt and its silencing is lethal. Like other arthropod cuticular proteins, Cq-M15 possesses a chitin-binding Rebers–Riddiford domain, with a recombinant version of the protein found to bind chitin. Cq-M15 was also found to interact with calcium ions in a concentration-dependent manner. This latter property might make Cq-M15 useful for bone and dental regenerative efforts. We suggest that, in the molar tooth, this protein might be involved in calcium phosphate and/or carbonate precipitation.

KEY WORDS: Biomineralization, Crustacean, RNAi, Calcium, Hydroxyapatite, Chitin

INTRODUCTION

Biomineralization, the biogenic formation of mineral deposits, plays a central role in the formation and hardening of exoskeletons and occurs in almost all eukaryal phyla, although the morphology and extent of biomineralization vary widely across species (Simkiss, 1975). Invertebrates deposit various mineral compositions, such as iron oxide (Lowenstam, 1967; Weaver et al., 2010), carbonate apatite (Currey et al., 1982; Lowenstam and Weiner, 1985, 1992), silica (van der Wal, 1989; Miller et al., 1990; Michels et al., 2012), protodolomite (Ma et al., 2008), amorphous calcium phosphate (ACP; Greenaway, 1985; Vijayan and Diwan, 1996; Levi-Kalisman et al., 2002; Luquet and Marin, 2004; Neues et al., 2007; Kunkel and Jercinovic, 2013; Huber et al., 2014) and crystalline hydroxyapatite (Weaver et al., 2012), to increase the hardness of exoskeletal working surfaces. In vertebrates, enamel serves this purpose (Lucas, 2004). The mandibles of the arthropod *Cherax quadricarinatus* (Bentov et al., 2012) contain an unusual crystalline enamel-like apatite layer which resembles vertebrate enamel in both composition and function (Bentov et al., 2012). The appearance of an enamel-like apatite layer in a crayfish molar and the similarities found in its mechanical properties to mammalian teeth suggest a possible case of convergent evolution as previously described in other species (Lowenstam and Weiner, 1992; Bentov et al., 2012; Weaver et al., 2012). The apatite layer is presented in the form of fluorapatite (FAP) and is mounted on chitin reinforced with amorphous calcium carbonate (ACC) (Bentov et al., 2012). The mineral composition of the molar continuously transforms from the FAP to ACP and from ACP to ACC (Bentov et al., 2012).

Unlike vertebrate teeth, the complex functional tooth structure of the crayfish develops quickly, and is shed and regenerated with each molt cycle (Shechter et al., 2008a; Tynyakov et al., 2015). The molt cycle in crustaceans can be divided into four major stages, whereas a new exoskeleton is assembled during pre-molt and post-molt and sclerotized and calcified during post-molt (Shechter et al., 2008b). During pre-molt, the new epicuticle and exocuticle are built beneath the old cuticle (Roer and Dillaman, 1984), but these layers do not calcify until post-molt (Travis, 1963; Travis and Friberg, 1963). Thus, the mineral deposition of epicuticle and exocuticle begins at post-molt together with endocuticle synthesis (Drach, 1939; Travis, 1963, 1965; Travis and Friberg, 1963). Unlike the exoskeleton, the crayfish molar is assembled and mineralized during pre-molt (Tynyakov et al., 2015). Similarly to crustacean cuticle, the process of crayfish molar formation is entirely extracellular and presumably controlled by proteins, lipids, polysaccharides, low-molecular weight molecules and calcium salts (Willis, 1987; Lowenstam and Weiner, 1989; Horst and Freeman, 1993; Luquet, 2012).

As in vertebrates (Fujisawa and Tamura, 2012), skeletal proteins also play vital roles in mineral formation in invertebrates (Glazer and Sagi, 2012; Luquet, 2012). Previous *in vitro* experiments identified crustacean proteins thought to be associated with calcium carbonate calcification (Nagasawa, 2011). In contrast to vertebrates, the mineral in crustaceans is precipitated on chitin, which forms their exoskeletal structural components. As such, many exoskeletal proteins contain chitin-binding domains (Tabor, 1986), such as chitin-binding domain 2 (Tellam et al., 1999) and the Rebers–Riddiford (R–R) consensus sequence (Karouzou et al., 2007), and/or interact with calcium carbonate. Three known forms of the R–R consensus sequence, RR-1, RR-2 and RR-3, have all been recognized in proteins (Andersen, 2000) and shown experimentally to bind chitin (Rebers and Riddiford, 1988). However, there remains

[1]Department of Life Sciences, Ben-Gurion University, PO Box 653, Beer-Sheva 84105, Israel. [2]National Institute for Biotechnology in the Negev, Ben-Gurion University, PO Box 653, Beer-Sheva 84105, Israel. [3]Department of Biotechnology Engineering, Ben-Gurion University, PO Box 653, Beer-Sheva 84105, Israel. [4]Israel Oceanographic and Limnological Research, Haifa 8511911, Israel.

*Author for correspondence (sagia@bgu.ac.il)

Received 27 April 2015; Accepted 4 September 2015

Journal of Experimental Biology (2015) 218, 3487-3498 doi:10.1242/jeb.123539

a lack of knowledge about the interactions of R–R sequence-containing proteins with chitin and minerals and their localizations in the exoskeleton.

In vertebrates, different proteins have been suggested to play important roles in the mineralization of bones and teeth (George and Veis, 2008). *In vivo* studies suggested that some of these proteins may influence enamel plasticity (deformation behavior) and morphology, as well as the mineral content of teeth (Robinson et al., 2004; Gruenbaum-Cohen et al., 2009). Accordingly, mineralization experiments revealed that recombinant versions of these proteins contribute to the regulation of the structure and configuration of mineral particles *in vitro* (Deshpande et al., 2010; Fang et al., 2011).

The aim of this study was to identify and characterize a novel protein from the crustacean molar by means of the transcript tissue expression pattern, *in vivo* silencing of the transcript, mineral precipitation and chitin-binding assays with a recombinant protein. While *in vivo* silencing of the transcript was lethal, a recombinant version of the protein was found to bind chitin and interact in calcium carbonate and hydroxyapatite precipitation kinetics in a concentration-dependent manner *in vitro*.

MATERIALS AND METHODS

Animals and molt

Cherax quadricarinatus (Von Martens 1868) males were grown in artificial ponds at Ben-Gurion University of the Negev, Beer-Sheva, Israel, under conditions described previously (Shechter et al., 2008a). Intermolt crayfish were held in individual cages and endocrinologically induced to enter pre-molt through removal of the X-organ–sinus gland (XO–SG) complex in the eyestalk or injection of ecdysone into the hemolymph (Shechter et al., 2005, 2007). Growth of the gastrolith (the calcium storage organ) during the molt cycle was non-invasively evaluated using X-ray in terms of the molt mineralization index (MMI: gastrolith width/crayfish carapace length), which is used as an accurate molt stage marker (Shechter et al., 2007). For all dissection procedures, crayfish were placed on ice for 5–10 min until they were anesthetized.

Purification of molar proteins

Inter-molt stage animals were endocrinologically induced as above and, 14 days later, their molar teeth were dissected at late pre-molt. Molars were pulverized in liquid nitrogen using a mortar and pestle and proteins extracted as previously described (O'Brien et al., 1991; Tynyakov et al., 2015). In brief, protein extract was obtained using 5 mol l^{-1} guanidine thiocyanate, 0.5 mol l^{-1} EGTA, 5 mmol l^{-1} Pipes, pH 7 (1:10, w:v), at room temperature for 5 h. The extract was centrifuged at 16,000 ***g*** for 5 min in an Eppendorf microfuge, and the supernatant was dialyzed against 10 mmol l^{-1} ammonium bicarbonate, pH 7.8, overnight at 4°C and concentrated using a Vivaspin 20 (MWCO 10,000; Vivascience).

Two-dimensional separation and visualization

The molar protein extract was separated in two dimensions as described previously (Arnott et al., 1998) with a few modifications. Briefly, for isoelectric focusing, an immobiline dry strip (11 cm, pH 3–10) was rehydrated and aligned on an isoelectric focusing tray. The molar protein extract was loaded adjacent to the anode, and voltage was applied for a total of 11.9 kV h. Following isoelectric focusing, the gel strip was equilibrated in a buffer containing 6 mol l^{-1} urea, 0.375 mol l^{-1} Tris-HCl, pH 8.8, 2% SDS and 20% glycerol, and incubated in 2% dithiothreitol for reduction following 8% iodoacetamide for alkylation. Then the strip was mounted on a 15% SDS-PAGE gel with the Tris/glycine running buffer system as described previously (Lucas, 2004). Spots were visualized with Coomassie Blue staining and the corresponding gel pieces were excised for mass spectrometry.

Mass spectrometry

After undergoing two-dimensional gel separation and visualization, proteins from molar extracts were trypsin (Gold Trypsin, Promega) digested, and the peptides were purified on a C18 column and dissolved in 0.1% formic acid. Nanoliquid chromatography and mass-spectrometry analysis were performed as described previously (Glazer et al., 2010) using a 75 µm internal diameter fused silica column, packed with C18 (NewObjective, Woburn, MA, USA) connected to an Eksigent nano-LC system (Eksigent, Dublin, CA, USA). Mass spectra were acquired using an LTQ-Orbitrap XL (Thermo Fisher Scientific, San Jose, CA, USA) and analyzed using the PEAKS Mass Spectrometry Software, including a *de novo* peptide sequencing approach. Further Cq-M15 protein validation was performed by the Sequest and Mascot algorithms operated under Proteome Discoverer 2.0 (Thermo Fisher Scientific) using an NCBI database containing the newly identified M15 sequence.

Transcript sequencing

Degenerative primers Cq-M15 dF (5′-CAY TTY ACN GCN YTI WSI GC-3′) and Cq-M15 dR (5′-CGN CGN ATR GGY GGYGGY GG-3′) were generated based on the sequence of a partial fragment of *Cq-M15* obtained by tandem mass spectrometry. A fragment of the cDNA was amplified using Cq-M15 dF as a forward primer and Cq-M15 dR as a reverse primer. The PCR conditions using the REDTaq ReadyMix™ PCR Reaction Mix (Sigma) were: 94°C for 3 min, followed by 30 cycles of 94°C for 30 s, 55°C for 30 s and 72°C for 3 min, followed by a final elongation step of 72°C for 10 min. The fragment was cloned into the pGEM-T Easy vector (Promega, Madison, WI, USA) and sequenced. 5′- and 3′-RACE (rapid amplification of cDNA ends) was carried out with the SMART rapid amplification of cDNA ends kit (Clontech), according to the manufacturer's protocol to obtain the entire sequence of *Cq-M15*.

Cq-M15 sequence data have been deposited in the GenBank™ Data Bank with accession number KF739426.

Bioinformatic analysis

The deduced amino acid sequence of the gene was obtained bioinformatically by the ExPASy Translate tool (Artimo et al., 2012). Signal peptide and phosphorylation sites were predicted using SignalP 4.0 (Petersen et al., 2011) and NetPhos 2.0 (He et al., 2005), respectively. Identification of putative domains in the deduced protein sequence was predicted by SMART (Schultz et al., 1998; Suderman et al., 2006) and Motif Scan (Suzuki et al., 2013) and its type by a CuticleDB server (Karouzou et al., 2007). Physico-chemical parameters of the Cq-M15 protein sequence, including molecular weight and amino acid composition, were predicted using the ProtParam tool (Fujisawa and Tamura, 2012). Secondary structure predictions were done by PSIPRED (Futahashi and Fujiwara, 2008).

Phylogenetic analysis

A search for homologous sequences to Cq-M15 (www.ncbi.nlm.nih.gov) was performed using BLAST, and phylogenetic analysis among arthropod sequences was performed by the neighbor-joining method (Saitou and Nei, 1987) using MEGA5 software (Andersen, 2000). Evolutionary distances were computed using the Poisson correction method (Lu et al., 2007) and are expressed as amino acid substitutions per site. All positions containing gaps and missing data were eliminated from the analysis.

Temporal and spatial transcription

To identify tissue-specific temporal and spatial expression of *Cq-M15*, RNA was extracted from the forming epithelia of cuticle, mandible, molar and basal segment tissues, as well as from the hepatopancreas, muscle and testis, using an EZ-RNA Total RNA Isolation Kit (Biological Industries, Beit Haemek, Israel), according to the manufacturer's protocol. First strand cDNA was generated with oligo (dT) 22 VN using expand RT (Roche Diagnostics). *Cq-M15* was amplified by means of PCR with REDTaq ReadyMix™ PCR Reaction Mix (Sigma; one cycle at 94°C for 1 min; 30 cycles at 94°C for 1 min, 55°C for 2 min, 72°C for 3 min; one cycle at 72°C for 10 min) with the Cq-M15F (5′-CAACATGAAGTCTATTGTAATGT-TGGC-3′) and Cq-M15R (5′-TGTTTCAAATAAAGTATATTGAACC-3′) primers. 18S rRNA was evaluated as the control as described previously (Glazer et al., 2010).

Journal of Experimental Biology

Journal of Experimental Biology (2015) 218, 3487-3498 doi:10.1242/jeb.123539

In silico confirmation of *Cq-M15* sequence and transcription pattern

Reference *C. quadricarinatus* transcriptome was constructed from sequencing of four sets of samples as described previously (Tynyakov et al., 2015): (1) RNA extracted from hypodermis-, gastrolith- and molar-forming epithelium sequenced by 100 bp paired-end sequencing (Illumina HiSeq2000, USA); (2) RNA extracted from molar- and gastrolith-forming epithelium from different molt stages (intermolt, early pre-molt, late pre-molt and post-molt), barcoded and sequenced by 50 bp single-end sequencing (Illumina HiSeq2000, USA); (3) RNA sequenced by 454 technology, as described by Glazer et al. (2013); and (4) RNA sequenced 'single pass' by Sanger technology (expressed sequence tags, ESTs) as described by Yudkovski et al. (2010). All sequences (also called 'reads') were *de novo* assembled with CLC Genomics Workbench 6.51 (CLC Bio, Aarhus, Denmark) using default parameters. The resulting contigs were submitted to a second assembly by CAP3, yielding a collection of putative transcripts regarded as the 'reference *C. quadricarinatus* transcriptome'. The 50 bp sequences from molar and gastrolith samples in different molting stages described above were aligned to the reference *C. quadricarinatus* transcriptome using STAR 2.3. For estimation of transcript expression levels, the number of sequences aligned to each transcript in each stage was counted, and further normalized to the total number of sequences in that stage. A statistical test for assessing the differences in expression among stages was carried out using DESeq (Anders and Huber, 2010). The *Cq-M15* sequence was searched against the reference transcriptome using BLAST, and the transcript with the highest score and lowest *e*-value was regarded as the *Cq-M15* transcript in different molt stages: inter-molt (pool of animals, N=1), early pre-molt (pool of animals, N=1), late pre-molt (two single animals and one pool, N=3) and post-molt (two single animals, N=2).

Cq-M15 silencing

Cq-M15 and *CqVg* (*C. quadricarinatus* vitellogenin) dsRNAs were synthesized as described previously (Rosen et al., 2010). For a preparatory short-term silencing experiment, inter-molt males (MMI=0; 5–10 g) were injected with 5 µg g^{-1} of *Cq-M15* dsRNA (N=5) or *CqVg* dsRNA (N=5). Four consecutive injections were given once a day. On the fifth day, the animals were dissected to isolate the cuticle- and molar-forming epithelia and testis. For long-term silencing, the experimental group (N=10) was injected daily with *Cq-M15* dsRNA, while the control group (N=10) was injected with *CqVg* dsRNA. In both experiments, the daily injections included 1 ng μl^{-1} ecdysone (Sigma) (Glazer et al., 2010) to induce molting, applied into the sinus of the first abdominal segment.

Quantitative real-time RT-PCR

RNA was extracted as described above from the testis and the forming epithelium of the molar and cuticle at the following molt stages: mid- and late pre-molt (N_1, N_2=9), early and late post-molt (N_3, N_4=4) and inter-molt (N_5=4). The same procedure was performed with experimental and control males (N_6, N_7=5) of the short-term preliminary *in vivo Cq-M15*-silencing experiment. First strand cDNA was generated by reverse transcription using random hexamer primers (VersoTMcDNA kit, Thermo Fisher Scientific). Relative quantification was performed with the following primers: Cq-M15 F (5′ATGTTGGCTCTGCTTGCTG-3′), Cq-M15 R (5′-TGGTGCTCCA-TAGGTTGTGA-3′) and Universal Probe Library Probe no. 83 (Roche). Relative quantification of *M15* transcript levels was obtained using the following primers: Cq-M15qPCR_F (5′ATGAATTACATCATCTGTGA-GGAACC-3′), Cq-M15qPCR_R (5′CAATGAGCACATAACAGCCCA-3′) and Probe TM FAM-CTTGATTTTTACTGCCGTTGACACACTGA-BBQ, especially designed by TIB MOLBIOL Synthese labor (Roche). *Cq-18S* (accession no. AF235966), used as the normalizing agent, was evaluated in all the experiments by real-time RT-PCR in similar conditions (Glazer et al., 2010).

Recombinant protein production

Because of the negligible amounts of Cq-M15 and difficulty of extraction from tissue samples, in order to elucidate Cq-M15 functions *in vitro*, recombinant Cq-M15 (rCq-M15) was produced and purified, and verified through western blot by GenScript (GenScript Inc., Piscataway, NJ, USA). In brief, *rCq-M15* was chemically synthesized, cloned into pUC57-Kan vector and expressed in *E. coli* BL21 (DE3) cells at 37°C with 200 rpm agitation. SDS-PAGE and western blot were used to detect protein expression.

Chitin-binding assay

A chitin-binding assay was performed as described previously (Inoue et al., 2001). Briefly, a solution of rCq-M15 was incubated with chitin powder and further successively washed starting with DDW and then with 0.2 mol l^{-1} NaCl and finally boiled for 10 min in 2% SDS, 20% (v/v) β-mercaptoethanol. The supernatant of each wash was electrophoresed on 15% SDS-PAGE. The bands were visualized by silver staining. Bovine serum albumin (BSA) served as a negative control.

Circular dichroism

Circular dichroism (CD) was conducted with a J750 spectropolarimeter (Jasco, Easton, MD, USA) equipped with a Peltier device. Spectra in the absence and presence of calcium were measured at pH 7.4 using a 0.1 cm optical path Suprasil quartz cuvette (Hellma, Müllheim, Germany) in 400 µl of 0.028 mmol l^{-1} rCq-M15 prepared in 0.1 mmol l^{-1} Hepes. Then, 12 µl calcium chloride solution (1 mol l^{-1}) was added such that a molar ratio of rCq-M15 to Ca^{2+} ions of 1:1071 was obtained. Spectra were collected at a wavelength range of 190–260 nm at ambient temperature with a bandwidth of 1 nm, scan speed of 10 nm^{-1} min^{-1} and time constant of 4 s. Each spectrum represents an average of five successive scans over the 190–260 nm wavelength range.

Mineral precipitation assays

Different concentrations of rCq-M15 were tested in a calcium carbonate precipitation kinetics assay as described previously (Inoue et al., 2001), with slight modifications. In brief, 100 µl of 22 mmol l^{-1} $NaHCO_3$, pH 8.7, was added to 20 µl rCq-M15 in DDW at different concentrations (57, 230 and 459 µmol l^{-1}), to which 100 µl of 22 mmol l^{-1} $CaCl_2$ was added. Addition of DDW instead of rCq-M15 served as a negative control (blank). Turbidity was measured at 570 nm with a spectrophotometer.

Apatite precipitation experiments were performed as described previously (Beniash et al., 2011), with slight modifications. First, rCq-M15 was dialyzed against DDW and concentrated to 3 mg ml^{-1} using a SpeedVac apparatus. Then, 100 mmol l^{-1} stock solution of $CaCl_2$ was added to 20 µl of different concentrations (308, 615, 923 and 1850 µmol l^{-1}) of the dialyzed rCq-M15 in DDW, and 100 mmol l^{-1} $(NH_4)_2HPO_4$ was added to yield final concentrations of 2.5 mmol l^{-1} Ca^{2+} and 1.5 mmol l^{-1} phosphate. Droplets (20 µl) of the solution were placed on quartz slides in a humidity chamber for incubation at 37°C overnight at 100% humidity. In addition, 20 µl droplets of rCq-M15 at 923 µmol l^{-1} were placed on quartz slides in a humidity chamber for incubation at ambient temperature for 24 h and 2 weeks. After incubation, the quartz slides were dipped in DDW, air-dried and subjected to Raman spectroscopy. Raman spectra were acquired on a Jobin–Yvon LabRam HR 800 micro-Raman system equipped with a liquid nitrogen-cooled detector as described previously (Bentov et al., 2012).

Qualitative evaluation of the abundance of apatite and its precursor octacalcium phosphate (OCP) was performed as described previously (Crane et al., 2006). Calcium phosphate precipitation was performed in solution by mixing 1 mol l^{-1} calcium chloride ($CaCl_2$) and 0.5 mol l^{-1} sodium phosphate (Na_2HPO_4, NaH_2PO) (the two salts were used in different ratios to adjust the pH to 7.4) in 1.5 ml reaction volume, to a final concentration of 20 and 10 mmol l^{-1}, respectively. The precipitation assay was performed in the presence of 150 nmol l^{-1} or 4.1 µmol l^{-1} BSA, and 620 nmol l^{-1} or 3.1 µmol l^{-1} rCq-M15. All the reactions were performed in duplicate and were compared with the control (without the addition of protein). Each tube was loaded first with $CaCl_2$, H_2O (adjust to the volume of 1.5 ml) and the tested protein in the final desired concentration. Then, the Na_2HPO_4/NaH_2PO_4 solution was added to start the precipitation. After 24 h of incubation, the samples were centrifuged at 10,000 rpm and the pellet was separated and washed with DDW and centrifuged again. The pellet was than smeared on Opal slides (for low background) and allowed to dry completely. Samples were analyzed using Raman spectroscopy and

Journal of Experimental Biology (2015) 218, 3487-3498 doi:10.1242/jeb.123539

qualitative evaluation of the abundance of apatite and its precursor (OCP) was performed by subtracting the intensity of the 1010 cm^{-1} peak from the main PO_4 υ1 vibration of 960 cm^{-1}. Micro-Raman analyses of specimens were performed on a multichannel bench Renishaw InVia Reflex spectrometer (Renishaw InVia Raman, UK) coupled with a Peltier-cooled CCD detector. Excitation was provided by the 785 nm line of a diode laser. The samples were scanned from 200 to 1200 cm^{-1} wavenumber shift at a spectral resolution of 2 cm^{-1}. The scattered light was analyzed by a spectrograph with holographic grating (600 g mm^{-1}), slit width 150 mm and opened confocal hole (1000 mm). The time of acquisition of a particular spectral window was 10 s.

Statistical analysis

Data are expressed as means±s.e. Non-parametric tests were used as follows: statistical analysis for relative transcript levels among different tissues and molt stages, differences in survival rates after silencing with *Cq-M15* dsRNA and changes in turbidity of calcium carbonate precipitation with rCq-M15 final concentrations, as well as for qualitative evaluation of the apatite abundance, was performed using the Kruskal–Wallis rank sum test, followed by multiple pair-wise comparisons using the Wilcoxon rank sum test (with Bonferroni correction) for a two-sided test of significance. $P<0.05$ was considered statistically significant.

RESULTS

Identification, sequencing, bioinformatics analysis and biophysical characterization of Cq-M15

Initially, efforts were directed at defining the protein content of *C. quadricarinatus* molars. Separation of EGTA-extracted molar proteins by two-dimensional PAGE revealed the presence of at least 12 distinct spots. These spots were excised from the gel and subjected to mass spectrometry for peptide *de novo* sequencing. Degenerate primers corresponding to the obtained peptide sequences were constructed. Then, cDNA fragments were amplified and eventually full transcripts were obtained. While screening the protein profile of the molar tooth, a protein termed Cq-M15 was identified as a spot of ∼17 kDa and pI of ∼5.4 (Fig. S1, circled spot, modified) (Tynyakov et al., 2015). Its deduced 740 bp transcript includes a 5′ UTR of 18 bp, an ORF of 465 bp encoding a deduced 155 amino acid protein, and a 3′ UTR of 257 bp (Fig. 1). The first 15 amino acids are predicted to be a signal peptide. A chitin-binding R–R domain is suggested for residues 53–113. This domain is assigned to the RR-1 family, members of which have been found in soft and flexible cuticles (Kim et al., 2005). The predicted pI of Cq-M15 is 5.2, and approximately 5.8% of the total amino acids of the protein correspond to possible phosphorylation sites. Amino acid composition analysis of Cq-M15, moreover, revealed an abundance of non-polar, aliphatic amino acids, as well as polar but uncharged amino acids (Table 1).

```
  1 actcgcaacacctgcaacatgaagtctattgtaatgttggctctgcttgctgtggcggtg  60
  1                 M  K  S  I  V  M  L  A  L  L  A  V  A  V    14
 61 gctgataagcgaccactcacaacctatggagcaccaggcccagcacctagtcatggacac 120
 15 A  D  K  R  P  L  T  T  Y  G  A  P  G  P  A  P  S  H  G  H   34
121 cagggaccccagatcgctatcatccgcgacgatcgagtacaccctgatgcccagggcctt 180
 35 Q  G  P  Q  I  A  I  I  R  D  D  R  V  H  P  D  A  Q  G  L   54
181 tactccttaaacttggagaccgaggacggtattgtgaggcaggagtctggcggccccggt 240
 55 Y  S  L  N  L  E  T  E  D  G  I  V  R  Q  E  S  G  G  P  G   74
241 ggtagtcaacagggctctgtcagcttcactttccctgatggacaagtatttgaccttaag 300
 75 G  S  Q  Q  G  S  V  S  F  T  F  P  D  G  Q  V  F  D  L  K   94
301 ttcgtcgccgacgccgccggctaccagccccaatcctccttcttgccagtggctcctgag 360
 95 F  V  A  D  A  A  G  Y  Q  P  Q  S  S  F  L  P  V  A  P  E  114
361 ttcccacatccaatccctcagttcgtactggaccagatcgcatttgccgctcaggaagac 420
115 F  P  H  P  I  P  Q  F  V  L  D  Q  I  A  F  A  A  Q  E  D  134
421 gctgcccgagcacgtggtgaagtcaggagtccatccccaagctatggcgctccctcaaaa 480
135 A  A  R  A  R  G  E  V  R  S  P  S  P  S  Y  G  A  P  S  K  154
481 taataagttttaatgtacagttggatctaccacagatgaattacatcatctgtgaggaac 540
    *
541 cacttgatttttactgccgttgacacactgaccatgacacactgtcatgagcaaggaagg 600
601 taaatgggctgttatgtgctcattggtattatttcatgtagaatgagtgtaaatagtttg 660
661 tcataatttataactgttcaacagtttgtgtttcaaataaagtatattgaaccaaaaaaa 720
721 aaaaaaaaaaaaaaaaaaaa
```

Fig. 1. Nucleotide sequence of *Cq-M15* cDNA and the deduced amino acids of the open reading frame. The 5′ and 3′ UTRs are highlighted in gray. The putative signal peptide at the N-terminus of the protein is underlined. The predicted chitin-binding R–R domain is marked in bold. Predicted phosphorylation sites are boxed. The asterisk indicates a stop codon.

Cq-M15 resembles crustacean cuticular proteins expressed in mineralized cuticles

Following the assembly of its sequence, the similarity of the putative Cq-M15 protein to other proteins in protein databases was assessed, revealing Cq-M15 to be similar to cuticular proteins found in crustaceans and insects (Table 2). Evolutionarily, the above proteins were divided into two clades (Fig. 2). Clade i includes Cq-M15 and cuticular proteins from the mineralized parts of crustacean cuticles and clade ii encompasses cuticular proteins expressed in the crustacean arthrodial cuticles (non-calcified and flexible cuticles) and cuticular proteins expressed in insects. From an evolutionary perspective, Cq-M15 is thus much closer to crustacean proteins from mineralized cuticles than to arthrodial and insect cuticles.

Cq-M15 transcription significantly differs as a function of tissue and molt stage

As suggested by its similarity to exoskeletal proteins from mineralized crustacean cuticles, and as the molar tooth is being built during pre-molt (Tynyakov et al., 2015), the specific expression of *Cq-M15* was tested in a number of target tissues at different molting stages. RT-PCR revealed that *Cq-M15* is transcribed at the mid- and late pre-molt stages in exoskeletal elements forming tissues, such as the cuticle, molar, basal segment, maxillae and gastrolith, as well as in non-exoskeletal tissue, such as the muscle, as compared with the transcription seen during inter-molt and post-molt (Fig. 3A). In most non-exoskeletal tissues,

Table 1. Physicochemical properties calculated for the Cq-M15 deduced protein sequence

	Amino acid	Cq-M15
Non-polar aliphatic	Gly	15 (9.7%)
	Ala	19 (12.3%)
	Val	11 (7.1%)
	Leu	10 (6.5%)
	Ile	7 (4.5%)
	Met	2 (1.3%)
	Total	64 (41.4%)
Aromatic	Phe	8 (5.2%)
	Tyr	4 (2.6%)
	Trp	0 (0.0%)
	Total	12 (7.8%)
Polar uncharged	Ser	13 (8.4%)
	Pro	17 (11.0%)
	Thr	4 (2.6%)
	Cys	0 (0.0%)
	Asn	1 (0.6%)
	Gln	12 (7.8%)
	Total	47 (30.4%)
Positively charged	Lys	4 (2.6%)
	His	4 (2.6%)
	Arg	7 (4.5%)
	Total	15 (9.7%)
Negatively charged	Asp	10 (6.5%)
	Glu	6 (3.9%)
	Total	16 (10.4%)

Amino acid composition is categorized according to side-chain properties. The percentage of amino acids corresponding to the total of each category is indicated in parentheses.

Journal of Experimental Biology

Journal of Experimental Biology (2015) 218, 3487-3498 doi:10.1242/jeb.123539

Table 2. Homology of full-length Cq-M15 to other arthropod cuticular proteins

Protein name	Animal	%Homology to Cq-M15 protein	NCBI accession no.
Calcification associated soluble matrix protein 2 (Casp 2)	*Procambarus clarkii*	52%	BAF73806.1
Strongly chitin-binding protein-1 (SCBP-1)	*Procambarus clarkii*	54%	BAM99303.1
Early cuticle protein 5 (ECP5)	*Callinectes sapidus*	58%	ADI59753.1
Early cuticle protein 6 (ECP6)	*Callinectes sapidus*	54%	ADI59754.1
Early cuticle protein 2 (ECP2)	*Callinectes sapidus*	50%	ADI59750.1
Early cuticle protein 1 (ECP1)	*Callinectes sapidus*	47%	ADI59749.1
Early cuticle protein 4 (ECP4)	*Callinectes sapidus*	47%	ADI59752.1
Early cuticle protein 3 (ECP3)	*Callinectes sapidus*	46%	ADI59751.1
Calcified cuticle protein CP14.1	*Callinectes sapidus*	54%	ABB91676.1
Arthrodial cuticle protein AMP16.5	*Callinectes sapidus*	42%	ABB91677.1
Arthrodial cuticle protein AMP16.3	*Callinectes sapidus*	42%	ABC26005.1
Arthrodial cuticle protein AMP8.1	*Callinectes sapidus*	37%	AAV28476.1
Cuticular protein CPR3	*Papilio xuthus*	36%	BAG30726.1
Cuticular protein RR-1 family member 40 precursor	*Nasonia vitripennis*	39%	NP_001161305.1
Cuticular protein RR-1 family member 19 precursor	*Nasonia vitripennis*	46%	NP_001161334.1
Cuticular protein RR-1 motif 6 precursor	*Bombyx mori*	48%	NP_001166742.1
Cuticular protein RR-1 motif 8	*Antheraea yamamai*	34%	AER27816.1
Pupal cuticle protein	*Culex quinquefasciatus*	46%	XP_001863934.1

including testes, no transcription was detected. RNA sequencing of hypodermis-, gastrolith- and molar-forming tissue by Illumina (560 million reads), and additional 454 and Sanger sequencing (287,900 reads) was followed by *de novo* assembly, yielding 56,490 contigs as described previously (Tynyakov et al., 2015). Based on the above database, a differential expression analysis of the *Cq-M15* transcript showed a significant increase (P<0.05) in normalized read count of early and late pre-molt compared with the post- and inter-molt

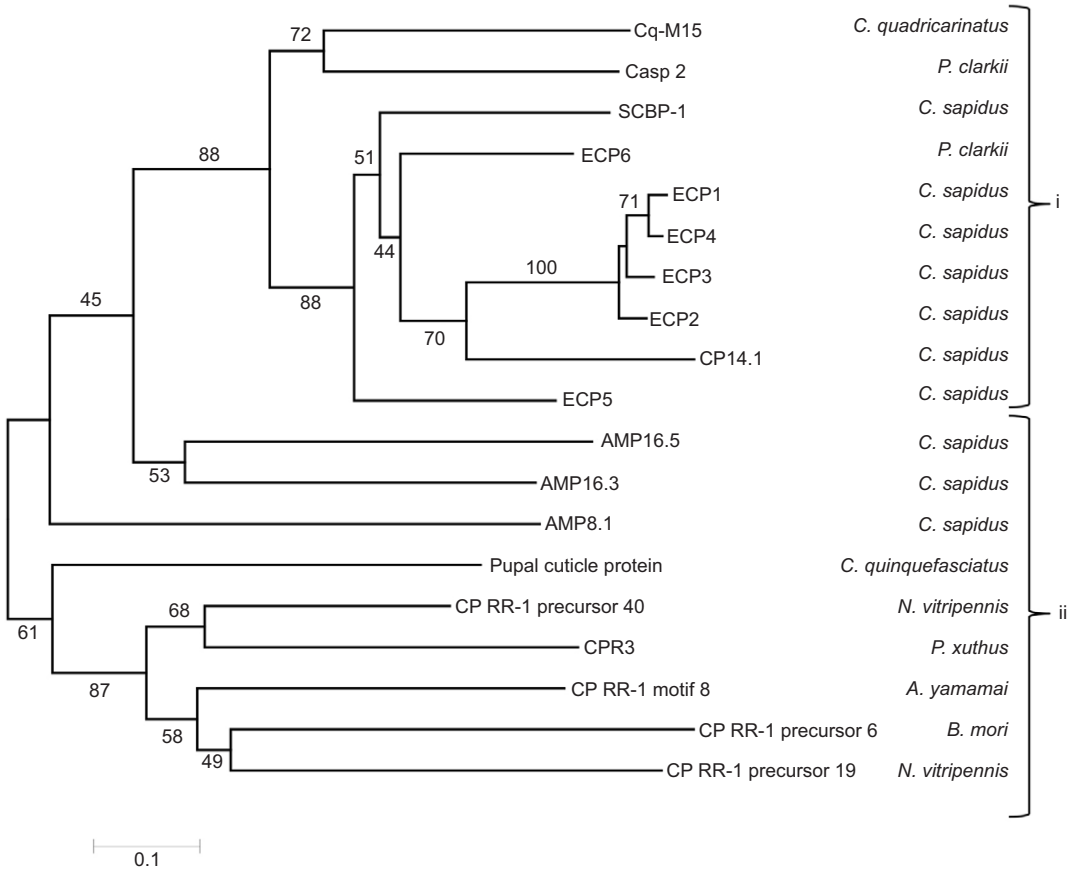

Fig. 2. Phylogenetic analysis of Cq-M15 in comparison to cuticular proteins from crustaceans and insects. The phylogenetic tree based on the *Cherax quadricarinatus* Cq-M15 protein sequence and those of homologous proteins from selected invertebrates (see Table 2) shows two distinct clades: one clade (i) comprises cuticular proteins (CP) from mineralized parts of cuticles and the second clade (ii) comprises cuticular proteins expressed in *arthrodial* cuticles of crustaceans and in insects. The numbers shown next to the branches indicate the percentage of replicate trees in which the associated taxa clustered together in the bootstrap test. The branch lengths correspond to evolutionary distances (expressed as the number of amino acid substitutions per site) used to infer the phylogenetic tree.

Journal of Experimental Biology (2015) 218, 3487-3498 doi:10.1242/jeb.123539

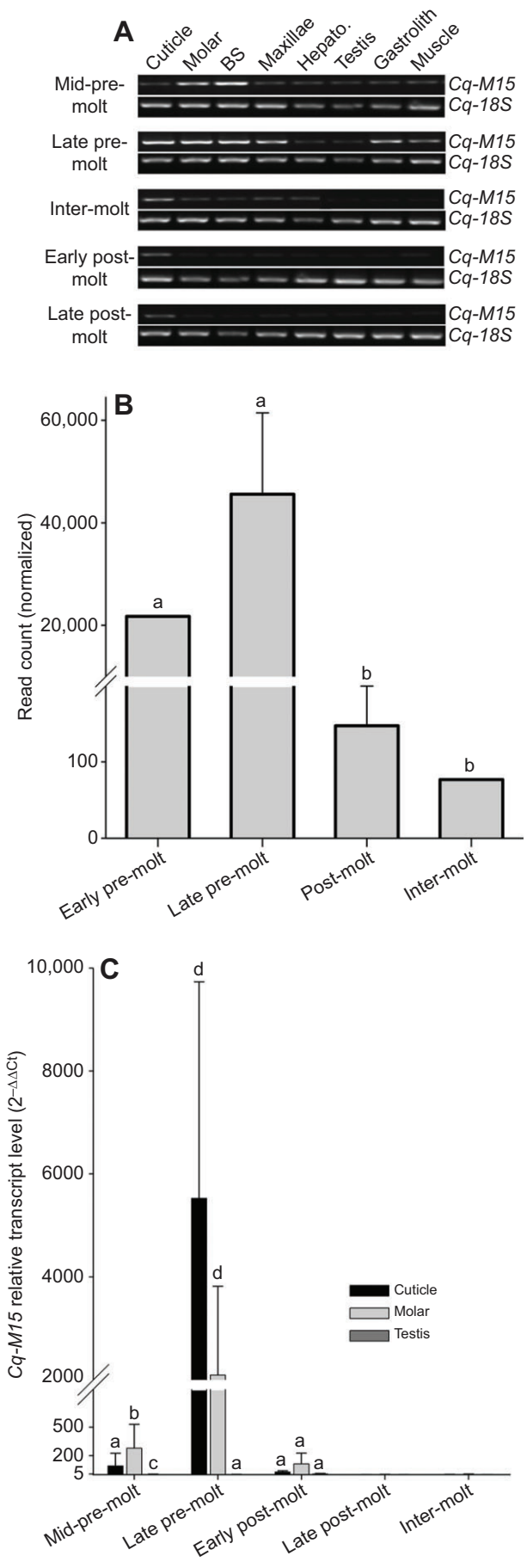

Fig. 3. Spatial and temporal expression patterns of the *Cq-M15* transcript *in vitro* and *in silico*. (A) Agarose gel electrophoresis of RT-PCR products demonstrates spatial and temporal expression patterns of the *Cq-M15* transcript in cuticle-, molar-, basal segment (BS)-, maxillae- and gastrolith-forming tissues, as well as in the hepatopancreas (Hepato.), testis and muscle. *Cq-18S* RNA was included as a control. (B) *In silico* transcriptomic analysis of Cq-M15 read counts from four different molt stages. Different letters above columns represent statistically significant differences (P<0.05). (C) Real-time RT-PCR-based relative quantification of *Cq-M15* transcript levels in the cuticle-, molar- and testis-forming tissues of crayfish injected with ecdysone. Error bars represent standard error. Different letters above columns represent statistically significant differences (P<0.05).

stages at the molar-forming epithelium samples as described in Fig. 3B. This was confirmed by real-time RT-PCR, which was performed next to evaluate differences in the relative transcription levels of *Cq-M15* between cuticle- and molar-forming tissues at different molt stages, with the level of transcript in testicular tissue serving as a control (Fig. 3C). The results show how *Cq-M15* transcription significantly differs as a function of tissue and molt stage (Kruskal–Wallis χ^2=79.3018, d.f.=14, P<0.001). Multiple pair-wise comparisons using the Wilcoxon rank sum test revealed that at mid-pre-molt, *Cq-M15* transcription in the molar-forming tissue was significantly higher than in cuticle-forming tissue (P<0.05), while such transcription in testis was significantly lower than in the latter (P<0.001). In late pre-molt, testicular tissue transcription of *Cq-M15* was significantly lower than in cuticle- and molar-forming tissues (P<0.001), while there was no significant difference between the latter two (W=60, P=0.09). Overall, *Cq-M15* transcription in cuticle- and molar-forming tissues at the late pre-molt stage was highest, relative to other molt stages (P<0.05). In contrast, *Cq-M15* was almost undetectable in the late post-molt and inter-molt stages (P<0.05).

In vivo injection of *Cq-M15* dsRNA causes a high mortality rate

As the expression of *Cq-M15* was significantly increased in relevant molt stages and locations related to exoskeleton and teeth assembly, a study of Cq-M15 function *in vivo* through an RNAi loss of function approach was attempted by *Cq-M15* dsRNA administration. First, the *Cq-M15* dsRNA sequence was compared with all known transcripts listed in *C. quadricarinatus* databases, in order to rule out non-specific silencing of non-*Cq-M15* transcripts in the crayfish (Yudkovski et al., 2007, 2010); no similar sequences were detected. The effectiveness of the RNAi-mediated gene knock-down was evaluated by qPCR (Fig. 4A). Examination of the relative quantification values obtained revealed significant differences between the experimental and the control groups (Kruskal–Wallis χ^2=24.6676, d.f.=5, P<0.001). When multiple pair-wise comparisons were conducted using the Wilcoxon rank sum test, a significantly lower level of *Cq-M15* transcription of the experimental group, compared with the control, was noted in the cuticle- and molar-forming tissues, as well as in testis (P<0.05).

Once the evaluation of the silencing effect of *Cq-M15* dsRNA injection had been established, a long-term silencing experiment addressing *Cq-M15* functionality was performed. This approach revealed a high mortality rate in the *Cq-M15* dsRNA-injected group (Fig. 4B). As such, the experiment was terminated after the death of the first seven experimental subjects, with no molt cycle differences noted between the groups. As *Cq-M15* was found to be transcribed at the pre-molt stage, the molt cycle was induced to initiate *Cq-M15* transcription. As the old exoskeleton does not

Journal of Experimental Biology (2015) 218, 3487-3498 doi:10.1242/jeb.123539

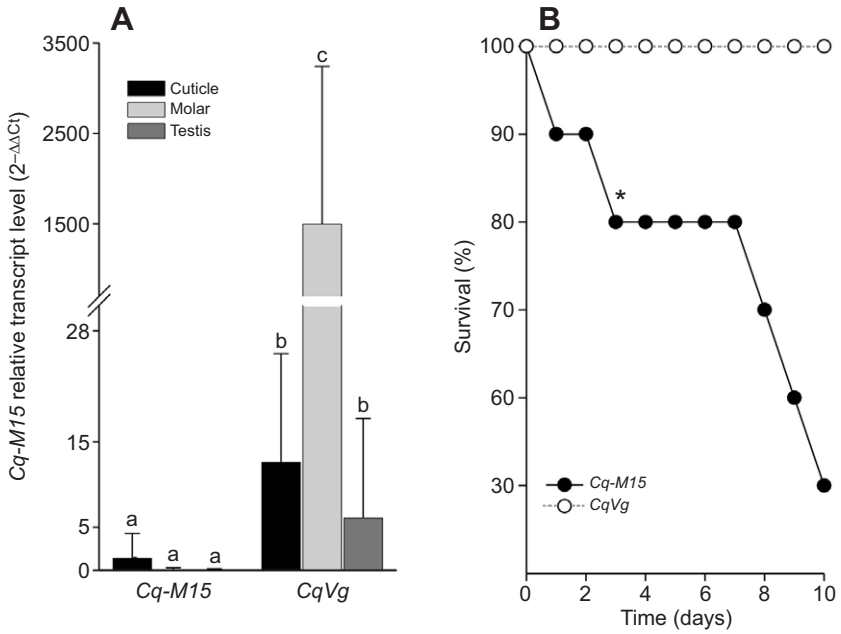

Fig. 4. Relative quantification of *Cq-M15* transcript levels. (A) Levels of *Cq-M15* transcript following *in vivo* dsRNA injections in male crayfish, as assessed by real-time RT-PCR following short-term silencing. The groups were injected with ecdysone to induce their molt cycle, and either *Cq-M15* dsRNA or *CqVg* dsRNA (control). Different letters represent significant differences (P<0.05) and error bars represent standard error. (B) Survival of *Cq-M15*-silenced *C. quadricarinatus* males. The groups were injected with ecdysone and *Cq-M15* or *CqVg* as described in A. The asterisk represents a significant difference (P<0.05).

undergo any changes during the newly induced molt cycle, the effects of silencing *Cq-M15* would be visible only at the newly formed exoskeleton. None of the experimental group crayfish built a new exoskeleton, including the molar. Thus, we could not perform any microscopic or spectral analysis of newly constructed molar morphology and composition. The rate of survival of the experimental group was 30% versus 100% for the control group (Fig. 4B), reflecting a significant difference starting from as early as the third day of the experiment (Wilcoxon rank sum test, W=2.5, P<0.05).

rCq-M15 possesses chitin-binding ability *in vitro*

rCq-M15 and BSA (which served as a control protein, lacking a chitin-binding domain; Shimizu et al., 1989) were separately incubated with chitin powder in *in vitro* studies to assess whether rCq-M15 binds to chitin. Unbound rCq-M15 and BSA were recovered in the supernatant after consecutive washes with DDW (Fig. 5, lanes 4 and 1 , respectively) and were also detected in the supernatant following further washing with weak salt solution (Fig. 5, lanes 5 and 2, respectively). After boiling the washed chitin in 2% SDS with 20% 2-mercaptoethanol, only rCq-M15 was recovered (Fig. 5, lane 6), indicating the strong binding of rCq-M15 to chitin, in accordance with the prediction of the presence of a chitin-binding domain.

rCq-M15 undergoes a conformational transition in the presence of Ca^{2+}

Evolutionary and sequence evidence point to the potential involvement of Cq-M15 in biomineralization, specifically in the precipitation of Ca^{2+} ions and its carbonate and phosphate salts. Thus, the interaction of rCq-M15 with Ca^{2+} ions and its carbonate and phosphate salts found in the mandible and molar tooth were next tested *in vitro*. Initially, rCq-M15 was assessed by CD. According to bioinformatics predictions, the first 96 residues of Cq-M15 contain a mixture of well-spaced loops and short β-sheets, whereas the region spanning residues 120–140 is predicted to fold as an α-helix. The CD curve obtained in calcium-free solution is characterized by minima at 213 and 216 nm (Fig. 6). In the presence of calcium, rCq-M15 undergoes a conformational transition, reflected by the appearance of prominent absorbance shoulders at 209, 215 and 218 nm.

rCq-M15 is involved in the enhancement of calcium carbonate precipitation rate *in vitro*

Finally, to investigate the role of Cq-M15 in the biomineralization processes, *in vitro* calcium carbonate and phosphate precipitation assays were conducted with rCq-M15. No significant differences between calcium carbonate precipitation rates were noted in the absence of rCq-M15 (blank, control) and in its presence at concentrations of 57 and 230 µmol l^{-1}. However, rCq-M15 at a concentration of 459 µmol l^{-1} significantly promoted calcium carbonate precipitation. At the end of the experimental period, the

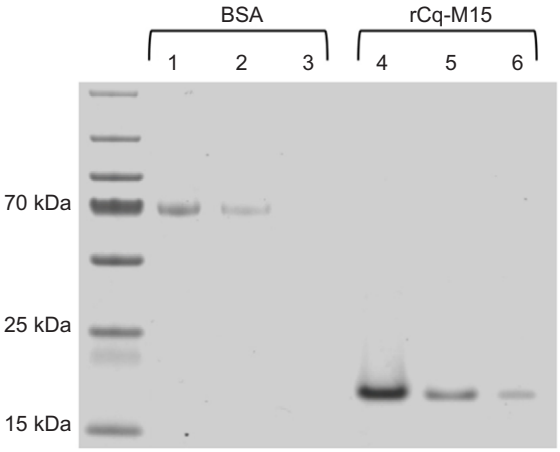

Fig. 5. Chitin-binding ability of rCq-M15. Following incubation of equal amounts of rCq-M15 and BSA with chitin powder, three consecutive washes were performed prior to SDS-PAGE. Lane 1 contains non-bound BSA after washing with DDW, lane 2 contains BSA after washing with 0.2 mol l^{-1} NaCl, and lane 3 contains BSA obtained after boiling in SDS/2-mercaptoethanol. Lane 4 contains non-bound rCq-M15 after washing with DDW, lane 5 contains rCq-M15 after washing with 0.2 mol l^{-1} NaCl and lane 6 contains rCq-M15 obtained after boiling in SDS/2-mercaptoethanol.

Journal of Experimental Biology (2015) 218, 3487-3498 doi:10.1242/jeb.123539

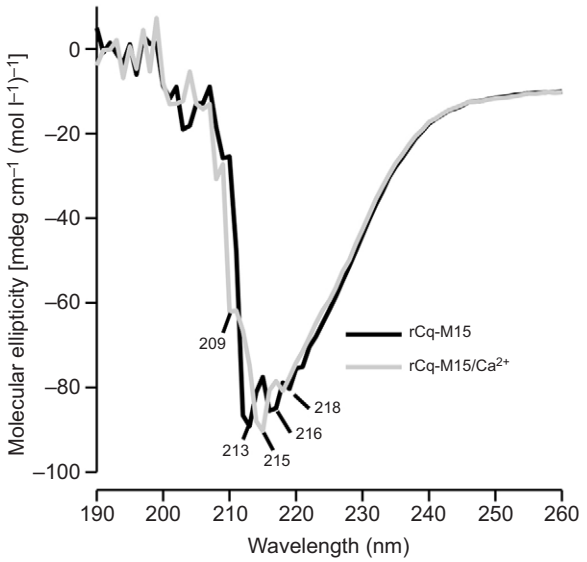

Fig. 6. Circular dichroism analysis of rCq-M15. The absorbance profiles of rCq-M15 in 0.1 mmol l^{-1} Hepes or in 0.1 mmol l^{-1} Hepes with $CaCl_2$ (1:1071 molar ratio of protein:Ca) are shown.

amount of deposited mineral (indicated by the absorbance) was shown to be concentration dependent with the blank showing the lowest value and 459 µmol l^{-1} rCq-M15 showing the highest (Wilcoxon rank sum test, $P<0.05$) (Fig. 7).

rCq-M15 is involved in the apatite precipitation process *in vitro*

With respect to calcium phosphate precipitation, rCq-M15 showed a concentration-dependent effect on hydroxyapatite precipitation at 37°C, compared with the blank (in the absence of rCq-M15), in which brushite (a hydroxyapatite precursor) (Park et al., 2002) was precipitated exclusively (Fig. 8A). At the initial concentration of 308 µmol l^{-1}, rCq-M15 precipitated brushite with characteristic Raman peaks at 904 and 990 cm^{-1} (Fig. 8A), while at a concentration of 615 µmol l^{-1}, rCq-M15 precipitated hydroxyapatite with a characteristic Raman peak at 960 cm^{-1} (Fig. 8A), indicative of the presence of both compounds in the precipitate. In the presence of 923 and 1085 µmol l^{-1} rCq-M15 (Fig. 8A), only the hydroxyapatite peak at 960 cm^{-1} was observed. To follow more realistic conditions of biomineralization in the crayfish, the above experiment was repeated for longer intervals and under ambient temperature. This experiment demonstrated that at a concentration of 923 µmol l^{-1}, rCq-M15 seems to interact in the kinetics of crystallization by enhancing the level of OCP (an additional precursor in the crystallization pathway of hydroxyapatite; Grynpas and Omelon, 2007), with a characteristic peak at 985 cm^{-1} at ambient temperature, compared with the blank in which brushite, with characteristic peaks at 904 and 990 cm^{-1}, was precipitated exclusively (Fig. 8B). In the presence of rCq-M15, OCP remained stable during the 2 week duration of the experiment (Fig. 8B), whereas in the blank, a mixture of brushite and OCP gradually appeared (Fig. 8B). Fig. 9 presents the numerical values of Raman intensity at 960 cm^{-1} (υ1 vibration of PO_4) after subtraction of the intensity of the 1010 cm^{-1} (typical OCP) peak. A significantly higher apatite/OCP ratio is shown in the presence of 3.1 µmol l^{-1} rCq-M15 compared with the control. No statistical difference in the apatite/OCP ratio was observed in the presence of 150 nmol l^{-1} or 4.1 µmol l^{-1} BSA.

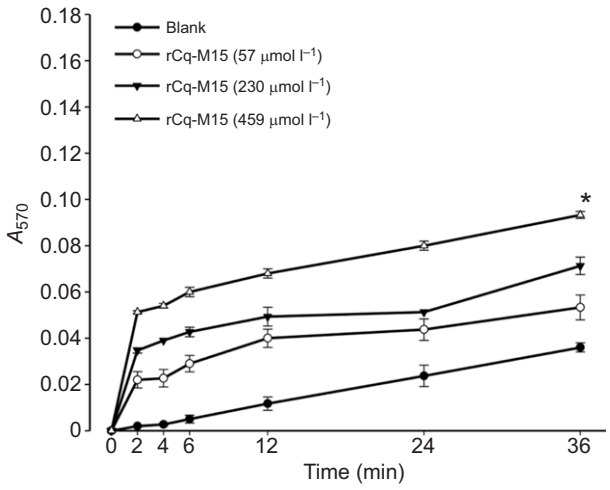

Fig. 7. Calcium carbonate precipitation in the presence of rCq-M15. Changes in the turbidity of a solution (measured by the absorbance at 570 nm, A_{570}) containing $NaHCO_3$ with different concentrations of rCq-M15 after addition of $CaCl_2$ are shown. The asterisk represents a significant difference ($P<0.05$).

DISCUSSION

In the present study, a novel protein termed Cq-M15 was identified from the crayfish molar tooth and found to be expressed in several exoskeleton-forming epithelia.

Characterization of the protein suggests its possible involvement in biomineralization. Indeed, this is the first report of an invertebrate protein suggested to interact in the precipitation of hydroxyapatite. The deduced protein sequence contains a predicted signal peptide, in accordance with the detection of the protein in the extracellular matrix. Cq-M15 has low percentages of acidic and putatively phosphorylated amino acids and possesses an RR1-type chitin-binding motif, which are more compatible with the properties of structural cuticular proteins (Willis, 2010) and, as such, do not favor an interaction with ions. However, Cq-M15 could be acidic enough to interact in mineral precipitation as has been discovered with other hydrophilic and acidic molecules involved in the regulation of crystal nucleation and growth during biological mineralization in vertebrates (He et al., 2005; Gayathri et al., 2007), as well as in invertebrates (Glazer and Sagi, 2012; Luquet, 2012). Moreover, several crustacean proteins associated with calcification processes present amino acid composition profiles similar to that of Cq-M15 (Inoue et al., 2004; Glazer et al., 2010). In fact, such shared patterns of amino acid composition were also found in proteins from organic matrices involved in invertebrate calcium carbonate precipitation (Faircloth and Shafer, 2007; Gayathri et al., 2007; Marie et al., 2007; Inoue et al., 2008; Suzuki et al., 2013), as well as in protein extracted from vertebrate enamel (Robinson et al., 2005).

The expression of *Cq-M15* during the pre-molt stage coincides with molar tooth mineralization and the synthesis of the new cuticle during this particular molt stage (Tynyakov et al., 2015) and presumably indicates the involvement of Cq-M15 in exoskeleton assembly and, specifically, in the early calcification of the molar tooth and other exoskeletal elements. Elevation of *Cq-M15* transcript expression in molar-forming epithelium at mid-pre-molt coincides with the formation of the apatite part (Tynyakov et al., 2015), which could implicate Cq-M15 interaction in calcium phosphate precipitation. Folowing the molt cycle progression, the highest *Cq-M15* expression was detected at late pre-molt both in molar- and cuticle-forming epithelium, which coincides with

Journal of Experimental Biology (2015) 218, 3487-3498 doi:10.1242/jeb.123539

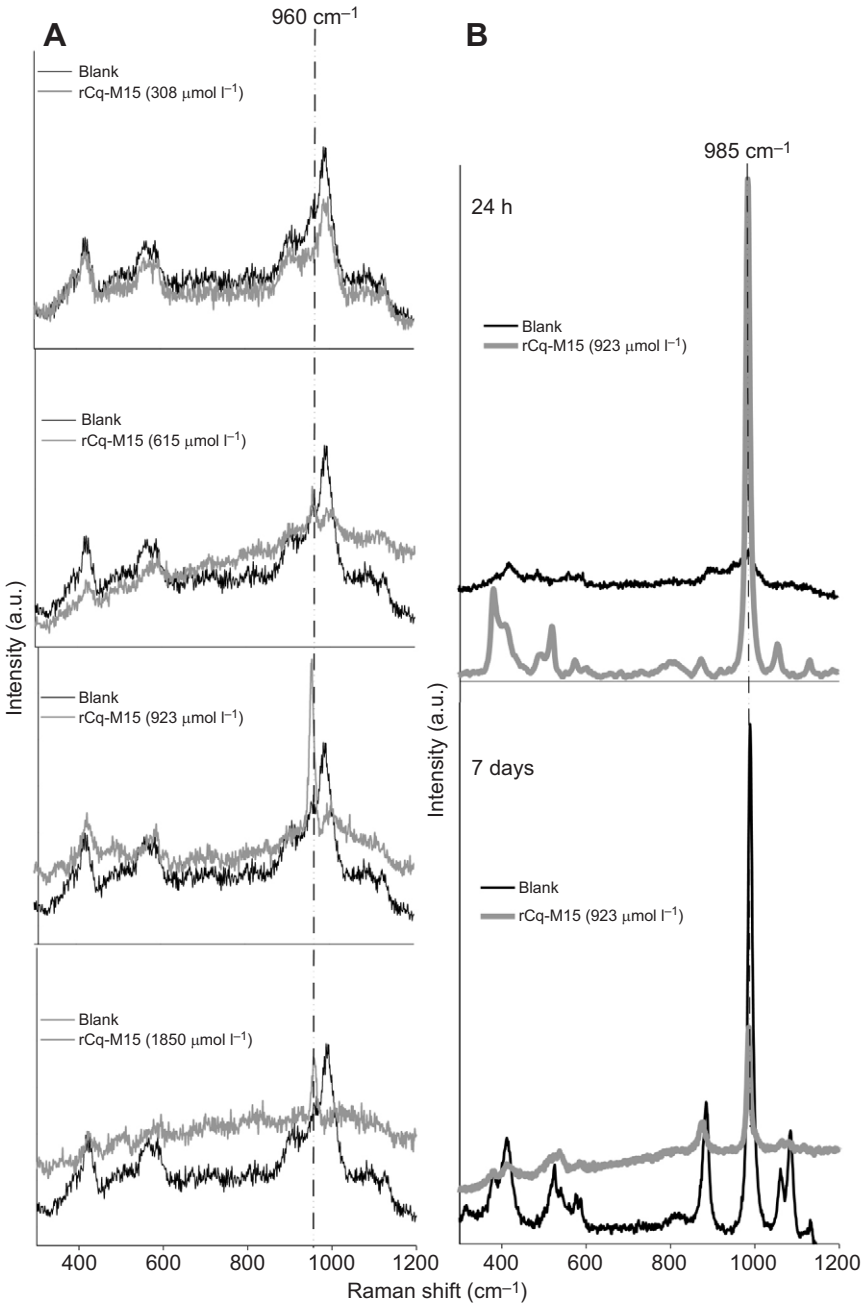

Fig. 8. Calcium phosphate precipitation in the presence of rCq-M15. (A) Raman spectra of the calcium phosphate phases that precipitate in the presence of different concentrations of rCq-M15 at 37°C (gray trace). The mineral precipitated (brushite) with no addition of protein is shown as a control (black trace). The peak of the hydroxyapatite is at 960 cm^{-1}, while that of brushite is at 990 cm^{-1}. An additional peak of brushite at 904 cm^{-1} is typical for those phases that contain HPO_4 groups because of the P–O–H^+ configuration (usually between 875 and 925 cm^{-1}). (B) Raman spectra of the calcium phosphate phases that precipitate in the presence of 923 μmol l^{-1} rCq-M15 at 24°C, at 24 h (top) and 7 days (bottom; gray trace). The mineral precipitated with no addition of protein is shown as a control (black trace). The peak of brushite is at 990 cm^{-1}, octocalcium phosphate (OCP) is at 985 cm^{-1} and hydroxyapatite is at 960 cm^{-1}, with an additional peak of brushite at 904 cm^{-1} as in A. a.u., arbitrary units.

exocuticle synthesis (Drach, 1939; Roer and Dillaman, 1984). The latter could indicate the presence Cq-M15 in exocuticle and its interactions in calcium carbonate and ACC precipitation. We assume that in the molar, Cq-M15 is secreted by epithelial cells, the extensions of which presumably form an array of channels within the apatite layer (Bentov et al., 2012).

Cq-M15 is transcribed in muscle as well. Previously it was published that crustacean muscle growth is associated with the molt cycle. Previous studies have demonstrated that muscle protein synthesis rate is elevated during pre-molt (Mykles and Skinner, 1982; El Haj and Houlihan, 1987). Together with the protein synthesis elevation, claw muscles have been shown to undergo atrophy (Skinner, 1965; Mykles and Skinner, 1982), which enables the claw to be drawn through the narrow basi-ischium joint (Mykles and Skinner, 1990). It was beyond the scope of this study to investigate the relationship between *Cq-M15* expression, muscle type and changes in muscle through the molt cycle. However, based on the published literature, we would suggest the possible involvement of Cq-M15 in atrophy and restoration of muscle proteins to facilitate withdrawal from the carapace during molting.

The newly identified Cq-M15 was found to share significant similarity with known proteins from arthropod cuticles and its sequence was more closely related to crustacean proteins from mineralized parts of the cuticle (Gosline, 1980; Inoue et al., 2008; Suzuki et al., 2013) and more distantly related to proteins found in crustacean non-mineralized arthrodial membranes (Gosline, 1980) and insect cuticles (Kim et al., 2005; Futahashi and Fujiwara, 2008; Werren et al., 2010). Such close homology further supports the involvement of Cq-M15 in biomineralization in the crayfish. Furthermore, *in vivo* silencing of *Cq-M15* was lethal, suggesting it has a vital function during the molt cycle. While numerous gene-

Journal of Experimental Biology (2015) 218, 3487-3498 doi:10.1242/jeb.123539

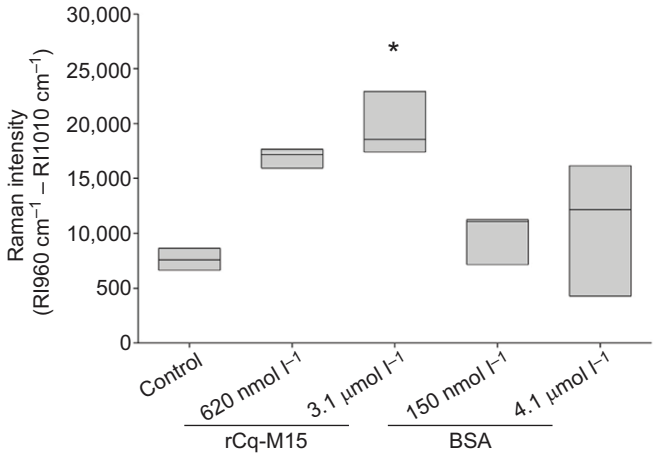

Fig. 9. Numerical evaluation of the apatite/OCP ratio in the presence of 620 nmol l^{-1} or 3.1 µmol l^{-1} rCq-M15. Boxes present the Raman intensity at 960 cm^{-1} (υ1 vibration of PO_4) after subtraction of the intensity at 1010 cm^{-1} (typical OCP peak). The results are compared with the apatite/OCP ratio in the presence of 150 nmol l^{-1} and 4.1 µmol l^{-1} BSA and with a control (without any protein). The lines represent median values and the asterisk represents a significant difference (P<0.05).

silencing studies assessing the functionality of novel crustacean genes have been published previously (Ventura et al., 2009, 2012; Rosen et al., 2010), to the best of our knowledge, the lethal effect of gene silencing has been previously reported in crustaceans only once (Christoffersen et al., 1989). We had shown earlier that silencing of particular transcripts in *C. quadricarinatus* affects the formation of the extracellular matrix and the calcification process (Shechter et al., 2008b; Glazer et al., 2010), as well as the duration of molt cycles (Pamuru et al., 2012; Tynyakov et al., 2015). However, the absence of the *C. quadricarinatus* sequenced genome does not permit us to completely rule out potential effects of non-specific small interfering RNAs derived from the *Cq-M15* sequence acting within target cells, even though a complete sequence search was done prior to the silencing study.

Cq-M15 is predicted to contain the RR1-type chitin-binding motif. However, unlike most such proteins found in soft cuticular elements, i.e. insect cuticles (Rebers and Riddiford, 1988), Cq-M15 was extracted from a hard exoskeletal organ, i.e. the molar tooth. This is thus only the second report of an RR1-type protein being present in a hard cuticle (Suderman et al., 2006). In accordance with the bioinformatics-based prediction, rCq-M15 chitin-binding ability suggests its direct association with the extracellular chitinous cuticular matrix in different parts of the crayfish exoskeleton. In accordance with computer modeling predicting that β-sheet folds of cuticular proteins form chitin-binding sites (Iconomidou et al., 2005), the ellipticity data obtained here confirmed the presence of β-sheets and a helical structure in rCq-M15. In addition, CD analysis revealed that Cq-M15 undergoes a conformational transition in the presence of calcium, possibly to provide the proper environment for mineral nucleation.

In vitro mineralization studies under conditions that support the spontaneous formation of calcium phosphate crystals (Margolis et al., 2006) suggest that Cq-M15 interacts in the processes of calcium carbonate and calcium phosphate crystal nucleation. ACP and/or OCP have been suggested as corresponding to precursor phases of apatite crystals in vertebrates (Grynpas and Omelon, 2007; Beniash et al., 2009) and invertebrates (Lowenstam and Weiner, 1985; Bentov et al., 2012; Weaver et al., 2012). As the ability of rCq-M15 to interact in the initiation of hydroxyapatite nucleation depends on temperature, it seems that additional physiological factors regulating the transition to hydroxyapatite, yet to be discovered in the crayfish molar apatite, might also be involved in this transition.

In conclusion, the data presented here suggest that Cq-M15 possesses physical traits that would allow it to play a role in molar tooth and cuticle biomineralization. Because transcript silencing was lethal, we could not demonstrate the involvement of Cq-M15 in ACP or AFP precipitation *in vivo*. *Cq-M15* spatial and temporal expression and its participation in mineral precipitation *in vitro* point to a possible role in calcium carbonate precipitation, including ACC precipitation. Thus, the above-discussed characteristics of Cq-M15 point to the involvement of the protein in the formation of the chitin–protein–mineral complex of the molar tooth and cuticle, through interactions with the chitinous matrix and calcium ions, and possibly with other proteins yet to be discovered. In addition, the level of the interaction depends in a concentration-dependent manner on the amount of calcium ions. Recombinant proteins that are produced in *E. coli* lack post-translational modification (Hannig and Makrides, 1998; Jonasson et al., 2002), and therefore we suppose that the Cq-M15 recombinant protein could possess a different tertiary and/or quaternary conformation compared with native Cq-M15 protein in the *in vitro* medium. Moreover, the Cq-M15 recombinant protein interacts in hydroxyapatite precipitation, whereas the molar is covered by fluoroapatite (Bentov et al., 2012), both of which are molecular forms of apatite but with a different *in vitro* conformation. Thus, this protein could be involved in calcium phosphate and/or carbonate precipitation. Further study of Cq-M15 properties and neighboring proteins will increase our knowledge on the involvement of proteins in exoskeletal calcified tissues and may prove instrumental for research in the fields of bone and teeth repair/regeneration and nano-structured materials.

Acknowledgements
We thank Leila Zeiri for technical assistance with Raman studies and Vered Chalifa-Caspi for her professional support in next generation sequencing analysis. Animals for the study were supplied by the Department of Fisheries and Aquaculture, Dor Agriculture Center.

Competing interests
The authors declare no competing or financial interests.

Author contributions
J.T. and A.S. designed the research; J.T., S.B. and S.W. performed the research; G.Y., Z.R., A.B. and I.K. contributed analytic tools; J.T., S.B., I.K., S.A., E.D.A., I.P., M.T. and A.S. analyzed the data; J.T. and A.S. wrote the paper.

Funding
This study was supported in part by grants from the Israel Science Foundation (ISF, grants 102/09 and 613/13) and the National Institute for Biotechnology in the Negev (NIBN).

Supplementary information
Supplementary information available online at
http://jeb.biologists.org/lookup/suppl/doi:10.1242/jeb.123539/-/DC1

References
Anders, S. and Huber, W. (2010). Differential expression analysis for sequence count data. *Genome Biol.* **11**, R106.
Andersen, S. O. (2000). Studies on proteins in post-ecdysial nymphal cuticle of locust, *Locusta migratoria*, and cockroach, *Blaberus craniifer*. *Insect Biochem. Mol. Biol.* **30**, 569-577.
Arnott, D., O'Connell, K. L., King, K. L. and Stults, J. T. (1998). An integrated approach to proteome analysis: identification of proteins associated with cardiac hypertrophy. *Anal. Biochem.* **258**, 1-18.
Artimo, P., Jonnalagedda, M., Arnold, K., Baratin, D., Csardi, G., de Castro, E., Duvaud, S., Flegel, V., Fortier, A., Gasteiger, E. et al. (2012). ExPASy: SIB bioinformatics resource portal. *Nucleic Acids Res.* **40**, W597-W603.

Beniash, E., Metzler, R. A., Lam, R. S. K. and Gilbert, P. U. P. A. (2009). Transient amorphous calcium phosphate in forming enamel. *J. Struct. Biol.* **166**, 133-143.
Beniash, E., Deshpande, A. S., Fang, P. A., Lieb, N. S., Zhang, X. and Sfeir, C. S. (2011). Possible role of DMP1 in dentin mineralization. *J. Struct. Biol.* **174**, 100-106.
Bentov, S., Zaslansky, P., Al-Sawalmih, A., Masic, A., Fratzl, P., Sagi, A., Berman, A. and Aichmayer, B. (2012). Enamel-like apatite crown covering amorphous mineral in a crayfish mandible. *Nat. Commun.* **3**, 839.
Christoffersen, J., Christoffersen, M. R., Kibalczyc, W. and Andersen, F. A. (1989). A contribution to the understanding of the formation of calcium phosphates. *J. Cryst. Growth* **94**, 767-777.
Crane, N. J., Popescu, V., Morris, M. D., Steenhuis, P. and Ignelzi, M. A. Jr. (2006). Raman spectroscopic evidence for octacalcium phosphate and other transient mineral species deposited during intramembranous mineralization. *Bone* **39**, 434-442.
Currey, J. D., Nash, A. and Bonfield, W. (1982). Calcified cuticle in the stomatopod smashing limb. *J. Mater. Sci.* **17**, 1939-1944.
Deshpande, A. S., Fang, P.-A., Simmer, J. P., Margolis, H. C. and Beniash, E. (2010). Amelogenin-collagen interactions regulate calcium phosphate mineralization in vitro. *J. Biol. Chem.* **285**, 19277-19287.
Drach, P. (1939). Mue et cycle d'intermue chez les Crustaces Decapodes. *Ann. Inst. Oceanogr* **19**, 103-391.
El Haj, A. J. and Houlihan, D. F. (1987). In vitro and in vivo protein synthesis rates in a crustacean muscle during the moult cycle. *J. Exp. Biol.* **127**, 413-426.
Faircloth, L. M. and Shafer, T. H. (2007). Differential expression of eight transcripts and their roles in the cuticle of the blue crab, *Callinectes sapidus*. *Comp. Biochem. Physiol. B Biochem. Mol. Biol.* **146**, 370-383.
Fang, P.-A., Conway, J. F., Margolis, H. C., Simmer, J. P. and Beniash, E. (2011). Hierarchical self-assembly of amelogenin and the regulation of biomineralization at the nanoscale. *Proc. Natl. Acad. Sci. USA* **108**, 14097-14102.
Fujisawa, R. and Tamura, M. (2012). Acidic bone matrix proteins and their roles in calcification. *Front. Biosci.* **17**, 1891-1903.
Futahashi, R. and Fujiwara, H. (2008). Identification of stage-specific larval camouflage associated genes in the swallowtail butterfly, *Papilio xuthus*. *Dev. Genes Evol.* **218**, 491-504.
Gayathri, S., Lakshminarayanan, R., Weaver, J. C., Morse, D. E., Kini, R. M. and Valiyaveettil, S. (2007). In vitro study of magnesium-calcite biomineralization in the skeletal materials of the seastar *Pisaster giganteus*. *Chem. Eur. J.* **13**, 3262-3268.
George, A. and Veis, A. (2008). Phosphorylated proteins and control over apatite nucleation, crystal growth, and inhibition. *Chem. Rev.* **108**, 4670-4693.
Glazer, L. and Sagi, A. (2012). On the involvement of proteins in the assembly of the crayfish gastrolith extracellular matrix. *Invertebr. Reprod. Dev.* **56**, 57-65.
Glazer, L., Shechter, A., Tom, M., Yudkovski, Y., Weil, S., Aflalo, E. D., Pamuru, R. R., Khalaila, I., Bentov, S., Berman, A. et al. (2010). A protein involved in the assembly of an extracellular calcium storage matrix. *J. Biol. Chem.* **285**, 12831-12839.
Glazer, L., Tom, M., Weil, S., Roth, Z., Khalaila, I., Mittelman, B. and Sagi, A. (2013). Hemocyanin with phenoloxidase activity in the chitin matrix of the crayfish gastrolith. *J. Exp. Biol.* **216**, 1898-1904.
Gosline, J. M. (1980). The elastic properties of rubber-like proteins and highly extensible tissues. *Symp. Soc. Exp. Biol.* **34**, 332.
Greenaway, P. (1985). Calcium balance and moulting in the Crustacea. *Biol. Rev.* **60**, 425-454.
Gruenbaum-Cohen, Y., Tucker, A. S., Haze, A., Shilo, D., Taylor, A. L., Shay, B., Sharpe, P. T., Mitsiadis, T. A., Ornoy, A., Blumenfeld, A. et al. (2009). Amelogenin in cranio-facial development: the tooth as a model to study the role of amelogenin during embryogenesis. *J. Exp. Zool. B Mol. Dev. Evol.* **312B**, 445-457.
Grynpas, M. D. and Omelon, S. (2007). Transient precursor strategy or very small biological apatite crystals? *Bone* **41**, 162-164.
Hannig, G. and Makrides, S. C. (1998). Strategies for optimizing heterologous protein expression in *Escherichia coli*. *Trends Biotechnol.* **16**, 54-60.
He, G., Ramachandran, A., Dahl, T., George, S., Schultz, D., Cookson, D., Veis, A. and George, A. (2005). Phosphorylation of phosphophoryn is crucial for its function as a mediator of biomineralization. *J. Biol. Chem.* **280**, 33109-33114.
Horst, M. N. and Freeman, J. A. (1993). *The Crustacean Integument: Morphology and Biochemistry*. Boca Raton, FL: CRC Press.
Huber, J., Fabritius, H.-O., Griesshaber, E. and Ziegler, A. (2014). Function-related adaptations of ultrastructure, mineral phase distribution and mechanical properties in the incisive cuticle of mandibles of *Porcellio scaber* Latreille, 1804. *J. Struct. Biol.* **188**, 1-15.
Iconomidou, V. A., Willis, J. H. and Hamodrakas, S. J. (2005). Unique features of the structural model of 'hard'cuticle proteins: implications for chitin–protein interactions and cross-linking in cuticle. *Insect Biochem. Mol. Biol.* **35**, 553-560.
Inoue, H., Ozaki, N. and Nagasawa, H. (2001). Purification and structural determination of a phosphorylated peptide with anti-calcification and chitin-binding activities in the exoskeleton of the crayfish, *Procambarus clarkii*. *Biosci. Biotechnol. Biochem.* **65**, 1840-1848.
Inoue, H., Ohira, T., Ozaki, N. and Nagasawa, H. (2004). A novel calcium-binding peptide from the cuticle of the crayfish, *Procambarus clarkii*. *Biochem. Biophys. Res. Commun.* **318**, 649-654.
Inoue, H., Yuasa-Hashimoto, N., Suzuki, M. and Nagasawa, H. (2008). Structural determination and functional analysis of a soluble matrix protein associated with calcification of the exoskeleton of the crayfish, *Procambarus clarkii*. *Biosci. Biotechnol. Biochem.* **72**, 2697-2707.
Jonasson, P., Liljeqvist, S., Nygren, P.-Å. and Ståhl, S. (2002). Genetic design for facilitated production and recovery of recombinant proteins in *Escherichia coli*. *Biotechnol. Appl. Biochem.* **35**, 91-105.
Karouzou, M. V., Spyropoulos, Y., Iconomidou, V. A., Cornman, R. S., Hamodrakas, S. J. and Willis, J. H. (2007). *Drosophila* cuticular proteins with the R&R Consensus: annotation and classification with a new tool for discriminating RR-1 and RR-2 sequences. *Insect Biochem. Mol. Biol.* **37**, 754-760.
Kim, B. Y., Park, N. S., Jin, B. R. and Lee, S. M. (2005). Molecular cloning and characterization of a cDNA encoding a novel cuticle protein from the Chinese oak Silkmoth, *Antheraea pernyi*. *Mitochondrial DNA* **16**, 397-401.
Kunkel, J. G. and Jercinovic, M. J. (2013). Carbonate apatite formulation in cuticle structure adds resistance to microbial attack for American lobster. *Mar. Biol. Res.* **9**, 27-34.
Levi-Kalisman, Y., Raz, S., Weiner, S., Addadi, L. and Sagi, I. (2002). Structural differences between biogenic amorphous calcium carbonate phases using X-ray absorption spectroscopy. *Adv. Funct. Mater.* **12**, 43-48.
Lowenstam, H. A. (1967). Lepidocrocite, an apatite aineral, and magnetite in teeth of chitons (Polyplacophora). *Science* **156**, 1373-1375.
Lowenstam, H. A. and Weiner, S. (1985). Transformation of amorphous calcium phosphate to crystalline dahillite in the radular teeth of chitons. *Science* **227**, 51-53.
Lowenstam, H. A. and Weiner, S. (1989). *On Biomineralization*. New York: Oxford University Press.
Lowenstam, H. A. and Weiner, S. (1992). Phosphatic shell plate of the barnacle *Ibla* (Cirripedia): a bone-like structure. *Proc. Natl. Acad. Sci. USA* **89**, 10573-10577.
Lu, Y., Ye, L., Yu, S., Zhang, S., Xie, Y., McKee, M. D., Li, Y. C., Kong, J., Eick, J. D., Dallas, S. L. et al. (2007). Rescue of odontogenesis in Dmp1-deficient mice by targeted re-expression of DMP1 reveals roles for DMP1 in early odontogenesis and dentin apposition in vivo. *Dev. Biol.* **303**, 191-201.
Lucas, P. W. (2004). *Dental Functional Morphology: How Teeth Work*. New York: Cambridge University Press.
Luquet, G. (2012). Biomineralizations: insights and prospects from crustaceans. *Zookeys* **176**, 103-121.
Luquet, G. and Marin, F. (2004). Biomineralisations in crustaceans: storage strategies. *Comp. Rend. Palev.* **3**, 515-534.
Ma, Y., Aichmayer, B., Paris, O., Fratzl, P., Meibom, A., Metzler, R. A., Politi, Y., Addadi, L., Gilbert, P. U. P. A. and Weiner, S. (2008). The grinding tip of the sea urchin tooth exhibits exquisite control over calcite crystal orientation and Mg distribution. *Proc. Natl. Acad. Sci. USA* **106**, 6048-6053.
Margolis, H. C., Beniash, E. and Fowler, C. E. (2006). Role of macromolecular assembly of enamel matrix proteins in enamel formation. *J. Dent. Res.* **85**, 775-793.
Marie, B., Luquet, G., De Barros, J.-P. P., Guichard, N., Morel, S., Alcaraz, G., Bollache, L. and Marin, F. (2007). The shell matrix of the freshwater mussel *Unio pictorum* (Paleoheterodonta, Unionoida). *FEBS J.* **274**, 2933-2945.
Michels, J., Vogt, J. and Gorb, S. N. (2012). Tools for crushing diatoms–opal teeth in copepods feature a rubber-like bearing composed of resilin. *Sci. Rep.* **2**, 465.
Miller, C. B., Nelson, D. M., Weiss, C. and Soeldner, A. H. (1990). Morphogenesis of opal teeth in calanoid copepods. *Mar. Biol.* **106**, 91-101.
Mykles, D. L. and Skinner, D. M. (1982). *Muscle Atrophy and Restoration During Molting*. TN, USA: Oak Ridge National Lab.
Mykles, D. L. and Skinner, D. M. (1990). Atrophy of crustacean somatic muscle and the proteinases that do the job. A review. *J. Crustac. Biol.* **10**, 577-594.
Nagasawa, H. (2011). Structure and function of matrix proteins and peptides in the biomineral formation in crustaceans. In *Molecular Biomineralization*, Vol. 52 (ed. W. E. G. Müller), pp. 315-329. Berlin: Springer.
Neues, F., Goerlich, R., Renn, J., Beckmann, F. and Epple, M. (2007). Skeletal deformations in medaka (*Oryzias latipes*) visualized by synchrotron radiation micro-computer tomography (SRμCT). *J. Struct. Biol.* **160**, 236-240.
O'Brien, J. J., Kumaril, S. S. and Skinner, D. M. (1991). Proteins of crustacean exoskeletons: I. Similarities and differences among proteins of the four exoskeletal layers of four brachyurans. *Biol. Bull.* **181**, 427-441.
Pamuru, R. R., Rosen, O., Manor, R., Chung, J. S., Zmora, N., Glazer, L., Aflalo, E. D., Weil, S., Tamone, S. L. and Sagi, A. (2012). Stimulation of molt by RNA interference of the molt-inhibiting hormone in the crayfish *Cherax quadricarinatus*. *Gen. Comp. Endocrinol.* **178**, 227-236.
Park, G. T., Lim, S. E., Jang, S. I. and Morasso, M. I. (2002). Suprabasin, a novel epidermal differentiation marker and potential cornified envelope precursor. *J. Biol. Chem.* **277**, 45195-45202.

Petersen, T. N., Brunak, S., von Heijne, G. and Nielsen, H. (2011). SignalP 4.0: discriminating signal peptides from transmembrane regions. *Nat. Methods* **8**, 785-786.
Rebers, J. E. and Riddiford, L. M. (1988). Structure and expression of a *Manduca sexta* larval cuticle gene homologous to *Drosophila* cuticle genes. *J. Mol. Biol.* **203**, 411-423.
Robinson, C., Connell, S., Kirkham, J., Shore, R. and Smith, A. (2004). Dental enamel—a biological ceramic: regular substructures in enamel hydroxyapatite crystals revealed by atomic force microscopy. *J. Mater. Chem.* **14**, 2242-2248.
Robinson, C., Connell, S., Brookes, S. J., Kirkham, J., Shore, R. C. and Smith, D. A. M. (2005). Surface chemistry of enamel apatite during maturation in relation to pH: implications for protein removal and crystal growth. *Arch. Oral. Biol.* **50**, 267-270.
Roer, R. and Dillaman, R. (1984). The structure and calcification of the crustacean cuticle. *Am. Zool.* **24**, 893-909.
Rosen, O., Manor, R., Weil, S., Gafni, O., Linial, A., Aflalo, E. D., Ventura, T. and Sagi, A. (2010). A sexual shift induced by silencing of a single insulin-like gene in crayfish: ovarian upregulation and testicular degeneration. *PLoS ONE* **5**, e15281.
Saitou, N. and Nei, M. (1987). The neighbor-joining method: a new method for reconstructing phylogenetic trees. *Mol. Biol. Evol.* **4**, 406-425.
Schultz, J., Milpetz, F., Bork, P. and Ponting, C. P. (1998). SMART, a simple modular architecture research tool: identification of signaling domains. *Proc. Natl. Acad. Sci. USA* **95**, 5857-5864.
Shechter, A., Aflalo, E. D., Davis, C. and Sagi, A. (2005). Expression of the reproductive female-specific vitellogenin gene in endocrinologically induced male and intersex *Cherax quadricarinatus* crayfish. *Biol. Reprod.* **73**, 72-79.
Shechter, A., Tom, M., Yudkovski, Y., Weil, S., Chang, S. A., Chang, E. S., Chalifa-Caspi, V., Berman, A. and Sagi, A. (2007). Search for hepatopancreatic ecdysteroid-responsive genes during the crayfish molt cycle: from a single gene to multigenicity. *J. Exp. Biol.* **210**, 3525-3537.
Shechter, A., Berman, A., Singer, A., Freiman, A., Grinstein, M., Erez, J., Aflalo, D. E. and Sagi, A. (2008a). Reciprocal changes in calcification of the gastrolith and cuticle during the molt cycle of the red claw crayfish *Cherax quadricarinatus*. *Biol. Bull.* **214**, 122-134.
Shechter, A., Glazer, L., Cheled, S., Mor, E., Weil, S., Berman, A., Bentov, S., Aflalo, E. D., Khalaila, I. and Sagi, A. (2008b). A gastrolith protein serving a dual role in the formation of extracellular matrix containing an amorphous mineral. *Proc. Natl. Acad. Sci. USA* **105**, 7129-7134.
Shimizu, S., Sabsay, B., Veis, A., Ostrow, J. D., Rege, R. V. and Dawes, L. G. (1989). Isolation of an acidic protein from cholesterol gallstones, which inhibits the precipitation of calcium carbonate in vitro. *J. Clin. Invest.* **84**, 1990-1996.
Simkiss, K. (1975). *Bone and Biomineralization*. London: Edward Arnold.
Skinner, D. M. (1965). Amino acid incorporation into protein during the molt cycle of the land crab, *Gecarcinus lateralis*. *J. Exp. Zool.* **160**, 225-233.
Suderman, R. J., Dittmer, N. T., Kanost, M. R. and Kramer, K. J. (2006). Model reactions for insect cuticle sclerotization: cross-linking of recombinant cuticular proteins upon their laccase-catalyzed oxidative conjugation with catechols. *Insect Biochem. Mol. Biol.* **36**, 353-365.
Suzuki, M., Sugisaka-Nobayashi, A., Kogure, T. and Nagasawa, H. (2013). Structural and functional analyses of a Strong Chitin-Binding Protein-1 (SCBP-1) from the exoskeleton of the crayfish *Procambarus clarkii*. *Biosci. Biotechnol. Biochem.* **77**, 361-368.
Tabor, D. (1986). *Indentation Hardness and its Measurement: Some Cautionary Comments*. Philadelphia, PA: American Society for Testing and Materials.
Tellam, R. L., Wijffels, G. and Willadsen, P. (1999). Peritrophic matrix proteins. *Insect Biochem. Mol. Biol.* **29**, 87-101.
Travis, D. F. (1963). Structural features of mineralization from tissue to macromolecular levels of organization in the decapod Crustacea. *Ann. N. Y. Acad. Sci.* **109**, 177-245.
Travis, D. F. (1965). The deposition of skeletal structures in the crustacea. 5. The histomorphological and histochemical changes associated with the development and calcification of the branchial exoskeleton in the crayfish, *Orconectes virilis* Hagen. *Acta Histochem.* **20**, 193-222.
Travis, D. F. and Friberg, U. (1963). The deposition of skeletal structures in the crustacea: Vi. Microradiographic studies of the exoskeleton of the crayfish *Orconectes virilis* Hagen. *J. Ultrastruct. Res.* **9**, 285-301.
Tynyakov, J., Bentov, S., Abehsera, S., Khalaila, I., Manor, R., Katzir Abilevich, L., Weil, S., Aflalo, E. D. and Sagi, A. (2015). A novel chitin binding crayfish molar tooth protein with elasticity properties. *PLoS ONE* **10**, e0127871.
van der Wal, P. (1989). Structural and material design of mature mineralized radula teeth of Patella vulgata (gastropoda). *J. Ultrastruct. Mol. Struct. Res.* **102**, 147-161.
Ventura, T., Manor, R., Aflalo, E. D., Weil, S., Raviv, S., Glazer, L. and Sagi, A. (2009). Temporal silencing of an androgenic gland-specific insulin-like gene affecting phenotypical gender differences and spermatogenesis. *Endocrinology* **150**, 1278-1286.
Ventura, T., Manor, R., Aflalo, E. D., Weil, S., Rosen, O. and Sagi, A. (2012). Timing sexual differentiation: full functional sex reversal achieved through silencing of a single insulin-like gene in the prawn, *Macrobrachium rosenbergii*. *Biol. Reprod.* **86**, 90.
Vijayan, K. K. and Diwan, A. D. (1996). Fluctuations in Ca, Mg and P levels in the hemolymph, muscle, midgut gland and exoskeleton during the moult cycle of the Indian white prawn, *Penaeus indicus* (Decapoda: Penaeidae). *Comp. Biochem. Physiol. A Physiol.* **114**, 91-97.
Weaver, J. C., Wang, Q., Miserez, A., Tantuccio, A., Stromberg, R., Bozhilov, K. N., Maxwell, P., Nay, R., Heier, S. T., DiMasi, E. et al. (2010). Analysis of an ultra hard magnetic biomineral in chiton radular teeth. *Materials Today* **13**, 42-52.
Weaver, J. C., Milliron, G. W., Miserez, A., Evans-Lutterodt, K., Herrera, S., Gallana, I., Mershon, W. J., Swanson, B., Zavattieri, P., DiMasi, E. et al. (2012). The stomatopod dactyl club: a formidable damage-tolerant biological hammer. *Science* **336**, 1275-1280.
Werren, J. H., Richards, S., Desjardins, C. A., Niehuis, O., Gadau, J., Colbourne, J. K. and **The Nasonia Genome Working Group**. (2010). Functional and evolutionary insights from the genomes of three parasitoid nasonia species. *Science* **327**, 343-348.
Willis, J. H. (1987). Cuticular proteins: the neglected component. *Arch. Insect Biochem. Physiol.* **6**, 203-215.
Willis, J. H. (2010). Structural cuticular proteins from arthropods: annotation, nomenclature, and sequence characteristics in the genomics era. *Insect Biochem. Mol. Biol.* **40**, 189-204.
Yudkovski, Y., Shechter, A., Chalifa-Caspi, V., Auslander, M., Ophir, R., Dauphin-Villemant, C., Waterman, M., Sagi, A. and Tom, M. (2007). Hepatopancreatic multi-transcript expression patterns in the crayfish *Cherax quadricarinatus* during the moult cycle. *Insect Mol. Biol.* **16**, 661-674.
Yudkovski, Y., Glazer, L., Shechter, A., Reinhardt, R., Chalifa-Caspi, V., Sagi, A. and Tom, M. (2010). Multi-transcript expression patterns in the gastrolith disk and the hypodermis of the crayfish *Cherax quadricarinatus* at premolt. *Comp. Biochem. Physiol. D Genomics Proteomics* **5**, 171-177.